Defect-Assisted Photoinduced Halide Segregation in Mixed-Halide Perovskite Thin Films

*Alex J. Barker[1, §, *], Aditya Sadhanala[2, §, *], Felix Deschler[2], Marina Gandini[1], Satyaprasad P. Senanayak[2], Phoebe M. Pearce[2], Edoardo Mosconi[4,5], Andrew J. Pearson[2], Yue Wu[3], Ajay Ram Srimath Kandada[1], Tomas Leitjens[1], Filippo De Angelis[4,5], Siân E. Dutton[2], Annamaria Petrozza[1, *] Richard H. Friend[2,*]*

[1]Center for Nano Science and Technology@PoliMi, Istituto Italiano di Tecnologia, via Giovanni Pascoli 70/3, 20133, Milan, Italy.

[2]Cavendish Laboratory, University of Cambridge, JJ Thomson Avenue, Cambridge, CB3 0HE, UK

[3]Chemistry Research Laboratory, Mansfield Road, Oxford, OX1 3TA

[4]Computational Laboratory for Hybrid Organic Photovoltaics (CLHYO), CNR-ISTM, via Elce di Sotto 8, I-06123 Perugia, Italy.

[5]Computation, Istituto Italiano di Tecnologia, Via Morego 30, 16163 Genova, Italy.

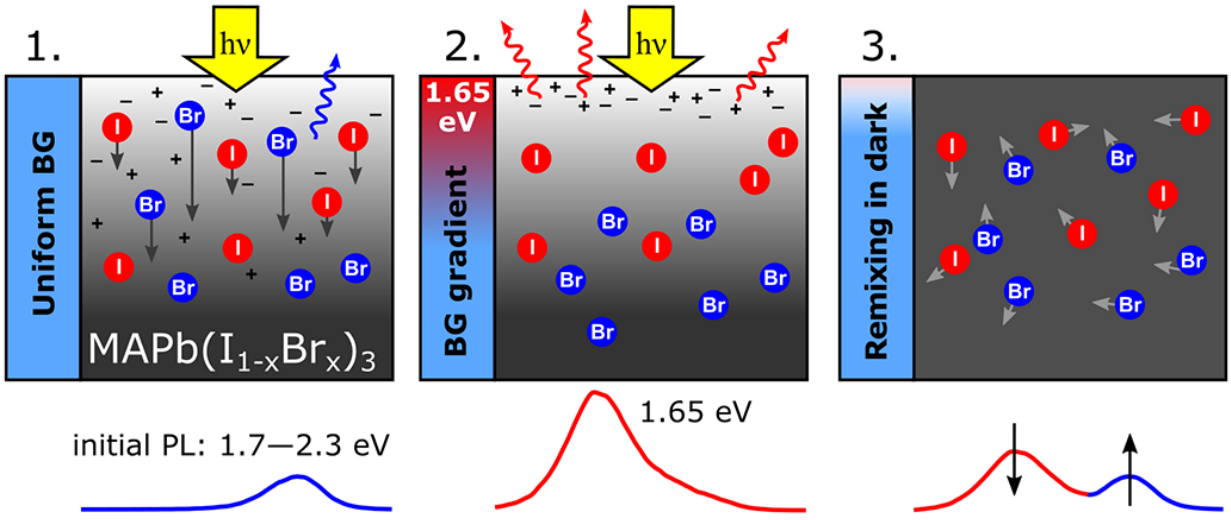
§ These authors have contributed equally.

[*]E-mail: alex.barker@iit.it (A.J.B.), as2233@cam.ac.uk (A.S.), annamaria.petrozza@iit.it(A.P.) and rhf10@cam.ac.uk (R.H.F.)

ABSTRACT

Solution processable organolead halide perovskites show immense promise for use in photovoltaics and other optoelectronic applications. The ability to tune their bandgap by alloying various halide anions (for example in $CH_3NH_3Pb(I_{1-x}Br_x)_3$, $0<x<1$) is however hampered by the reversible photoinduced formation of sub-bandgap emissive states. We find that ion segregation takes place via halide defects, resulting in iodide-rich low-bandgap regions close to the illuminated surface of the film. This segregation may be driven by the strong gradient in carrier generation rate through the thickness of these strongly absorbing materials. Once returned to the dark, entropically-driven intermixing of halides returns the system to a homogeneous condition. We present approaches to supress this process by controlling either the internal light distribution or the defect density within the film. These results are relevant to stability in both single- and mixed-halide perovskites, leading the way towards tuneable and stable perovskite thin films for photovoltaic and light-emitting applications.

TOC GRAPHIC



Organolead halide perovskite based solar cells have reached certified power conversion efficiencies (PCEs) exceeding 22%.[1] Additionally, these materials have been shown to demonstrate high photoluminescence quantum yields of more than 50% (at moderate carrier densities),[2] which led to reports on optically pumped lasing structures and light emitting devices (LEDs).[3,4]. The family of mixed-halide perovskites, $MAPb(I_{1-x}Br_x)_3$ ($MA = CH_3NH_3$, $0 \leq x \leq 1$), exhibit a continuously tuneable bandgap from 1.6 – 2.3 eV simply by adjusting the ratio of halide precursors,[5,6] with great appeal for application in multi-junction solar cells and tuneable light-emitting devices. However, when mixed-halide perovskites are employed as solar cell absorber layers, the maximum attainable open circuit voltage (V_{OC}) does not increase linearly with the change in the optical bandgap.[5,7] A subsequent study by Hoke *et al*[8] reported that white-light illumination induces formation of a strong and reversible sub-bandgap photoluminescence (PL) feature around 1.68 eV, independent of initial bandgap, which disappears after several minutes in the dark (hereafter referred to as the Hoke effect). That work, and subsequent others,[9–11] have attributed this behaviour to phase separation and the formation of iodide rich domains inducing low bandgap states. Additionally, mixed-halides using multiple A-site cations[12,13] or nanocrystalline morphology[14] display improved resilience to the Hoke effect, implying that the photoinduced changes are not necessarily an intrinsic phenomena of these materials. However, the mechanisms driving segregation and remixing, and the relative invariance of the sub-bandgap PL energy on initial material properties, are not yet fully understood.

Understanding the origin of the Hoke effect, and how to suppress it in operational devices, is complicated by the many parameters on which it depends. The rate of growth of the sub-bandgap PL has been shown to depend on the intensity and duty-cycle of illumination,[15,16] history of sample exposure,[17] sample pressure,[18] and the species of the A-site cation.[12,13] We show that the effect also depends on the internal light distribution within the material, which is not well explained by existing models of halide segregation, but is consistent with vertical

halide segregation. We consider that ion segregation takes place *via* halide defects, resulting in iodide-rich low-bandgap regions close to the illuminated surface of the film. This segregation is driven by the strong gradient in carrier generation rate through the thickness of these strongly absorbing materials. Once returned to the dark, entropically-driven intermixing of halides returns the system to a homogeneous condition.

Moreover, we demonstrate suppression of the Hoke effect in films engineered to experience a more homogeneous carrier generation profile, and produce stable mixed-halide films by controlling the density of halide defects, pointing the way towards photovoltaic and optoelectronic devices with a tuneable bandgap and stable V_{oc}. This result is also relevant to single-halide perovskites such as $MAPbI_3$, which exhibit slow photoinduced changes in optical[19] and electrical[20,21] behaviour associated with ion movement in the presence of charge carriers, but without the strong photoluminescent indicator of ion migration that is exhibited by these mixed-halide thin films.

Photoinduced sub-bandgap state formation

We use linear absorption to study the effect of white light exposure on the optical properties of $MAPb(I_{1-x}Br_x)_3$ films, where (unless otherwise stated) x refers to the ratio of the halide in the perovskite pre-cursor solutions. Figure 1a shows the photothermal deflection spectroscopy (PDS) spectra for iodide-bromide perovskite samples $MAPb(I_{1-x}Br_x)_3$ with x ranging from 0 to 1 before (lines), under (closed symbols), and after (open symbols) light soaking with intensity ~0.2 sun (see Figure S1 for the white light LED spectrum). Measurements on pure tri-iodide (x = 0) and tri-bromide (x = 1) show no evident change upon light soaking. In contrast, exposing mixed-halide (x = 0.4 or 0.6) perovskite films to light soaking for 10 minutes generates a low energy shoulder extending to ~ 1.65 eV, independent of initial halide ratio. Upon removal of light soaking, these features quickly reduce in intensity, and within 10 minutes the absorption returns to the initial spectrum measured prior to light exposure. The

absorbance levels of the defect shoulder (at ~ 1.65 eV) under light soaking for the solid solutions are about 5% of the absorbance at the band edges for both the x = 0.4 and x = 0.6 samples, indicating the formation of the observed sub-bandgap state in ~5% of the total sample. Impedance spectra of devices made with these materials also show a photoinduced feature, which is supressed at low temperatures (Figure S4). A third mixed-halide film with x = 0.6 was prepared using a 1.7× excess of the halide-bearing precursor solutions. PDS of the excess-halide film shows a higher energy band edge to the stoichiometric x = 0.6 film (likely due to to the preferential binding of Pb^{2+} and Br^- reported by Yoon et al[22]). More importantly, the absorption edge of the excess-halide film shows negligible change under light soaking.

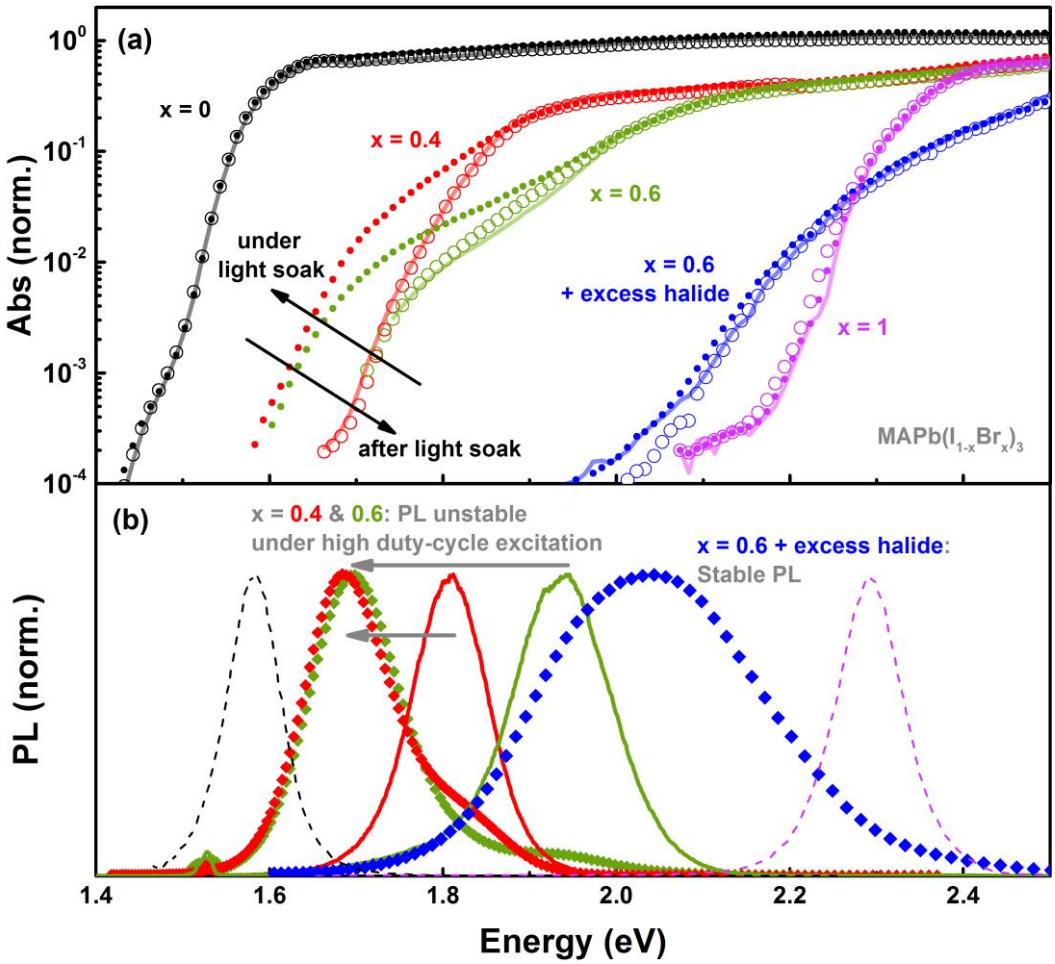


Figure 1: (a) PDS spectra for mixed-halide perovskite films, $MAPb(I_{1-x}Br_x)_3$ measured before (lines), under (closed symbols) and after (open symbols) light soaking (~0.2 sun). (b) PL spectra from excitation by low duty-cycle (solid lines) or high duty-cycle (diamonds) light pulses. PL spectra from single halide perovskites are shown in dashed lines for comparison.

It has been shown that the Hoke effect is more readily induced under continuous, rather than pulsed illumination,[16] implying that formation of the sub-bandgap state requires a sustained excited state population. Thus, by exciting the mixed-halide samples with either low duty-cycle (3.1 eV, 100 fs, 1 kHz, 1 μJ cm^{-2} $pulse^{-1}$) or high duty cycle (3.05 eV, 100 ps, 40 MHz, 46 pJ/cm^{-2} $pulse^{-1}$) light pulses, we collect the photoluminescence spectra associated with either the band-to-band or the photoinduced sub-bandgap emission respectively. Figure 1b shows that under high duty-cycle illumination, PL from the x = 0.4 and 0.6 samples is dominated by the sub-bandgap emission at 1.68 eV associated with the low-energy shoulder in absorption measured under light soaking. In contrast, PL from the excess-halide sample was found to be stable under changes in illumination duty cycle, consistent with the stable absorption profile shown under light soaking.

Figure 2a shows the growth of the sub-bandgap PL feature under illumination from light sources with three different wavelengths. The intensity of illumination was varied according to the absorption of the sample, to ensure a similar flux of absorbed photons in each case (experimental parameters are given in Table S1). Under illumination at 2.76 eV, well above the bandgap, growth of the PL feature is well characterised by a monoexponential with time constant τ = 4.6 s. As the excess energy is reduced, the feature emerges progressively more slowly (even though the absorbed photon flux is higher), with τ = 25 s under 2.33 eV illumination, and 55 s when excited at 1.95 eV, close to the optical bandgap. These changes in illumination wavelength determine not just the excess energy given to photogenerated charge carriers, but also the internal distribution of carrier generation rate throughout the depth of the film, as a result of the dependence of absorption coefficient on wavelength.[23] To decouple the role of hot carriers *vs* that of the internal light gradient, a beam splitter was used to provide excitation from either one of both sides of the sample (Figure 2b). After illumination from a single side had induced formation of the sub-bandgap feature, the addition of a second excitation source from the back of the sample resulted in a quenching of PL, even though the

total intensity of excitation was approximately doubled. This was accompanied by an increase of the mean PL energy, indicating a reduction in the efficiency of charge collection by iodide-rich regions under the more uniform charge generation profile.

If halide segregation requires a carrier generation gradient, the driving forces for segregation should be dependent on film opacity, and therefore thickness. We thus prepared both thick (280 nm) and thin (70 nm) films of $MAPb(I_{1-x}Br_x)_3$, with x = 0.85 (absorption, PL, and SEM in Figures S16 and S17). Figure 2c shows the changes in band-edge and sub-bandgap PL upon CW illumination (3.05 eV, 0.1 W cm^{-1}), normalised to the peak of the initial band-edge emission. While the difference in excitation conditions between the samples makes direct comparison difficult (the lower volume of the thinner film will result in higher carrier density, while an increased influence of surface traps may have the opposite effect), the pronounced differences in sub-bandgap PL behaviour still merit consideration. Both the growth rate and final amplitude of the sub-bandgap PL are much higher in the thick film, which absorbs >90% of the incident light. The thin film, which features the same absorption per unit thickness but only absorbs ~40% of the total light (resulting in a lower variation of carrier generation rate across the film) displays a much slower rise and lower intensity of sub-bandgap PL, with negligible quenching of the high-energy PL from the pristine (non-segregated) blend.

We now turn to structural and ultrafast optical analyses to understand the nature of the sub-bandgap states, the driving forces behind their formation (and relaxation), and why their emission energy is independent of the initial halide ratio.

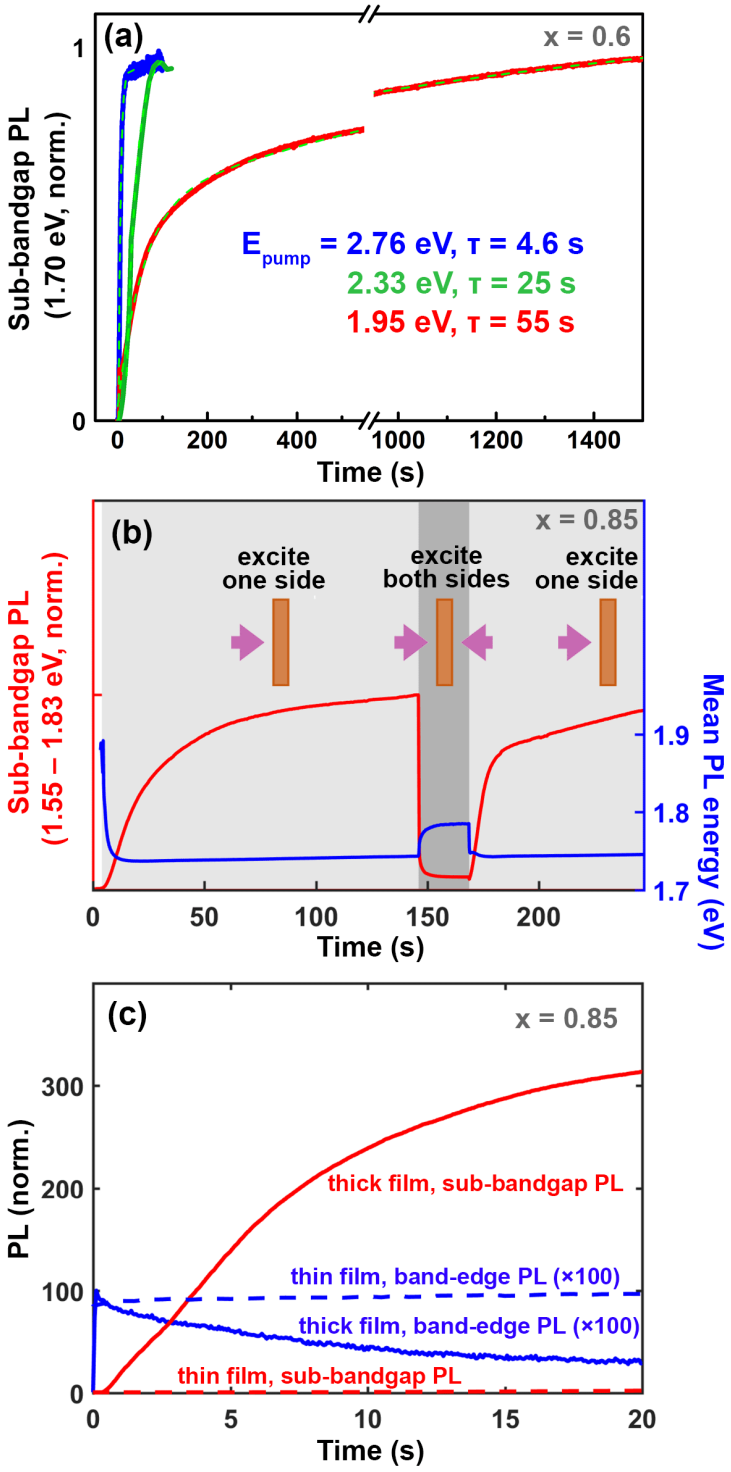


Figure 2: CW PL characterisations. (a) Excitation energy dependence of sub-bandgap PL growth of a 250 nm thick thin-film using three different CW laser excitation sources with comparable absorbed photon flux. (b) Dependence of sub-bandgap PL growth and mean PL energy on excitation geometry. (c) Dependence of photoinduced changes in PL on film thickness.

Photophysics of the photoinduced sub-bandgap states

The physical processes underpinning the Hoke effect occur over two distinct timescales: light induced halide segregation takes place over timescales of seconds, while the transport of photoinduced carriers from throughout the film to the iodide-rich (low-bandgap) regions occurs approximately eleven orders of magnitude more rapidly. In order to investigate both of these processes, we have conducted ultrafast transient absorption (TA) spectroscopy with and without light soaking. This pump-probe method is capable of tracking excited state dynamics taking place in our samples between photoexcitation and photoluminescence.

Figure 3a presents the evolution of the differential transmission in the absence of light soaking. The short excitation pulses enabled investigation of excited state processes without activating the sub-bandgap recombination pathway. Accordingly, the excited state behaviour closely resembles that of $MAPbI_3$ and $MAPbBr_3$ thin films (Figure S9). The signal is dominated by a ground-state bleach (GSB) due to occupation of excited-states near the band edge (in this case, centred around 2.16 eV, in agreement with absorption measurements), which can be taken as a measure for the photoinduced excited state density.[2,24] Additional spectral features within the first two picoseconds have been attributed to processes such as bandgap renormalization.[25–27]

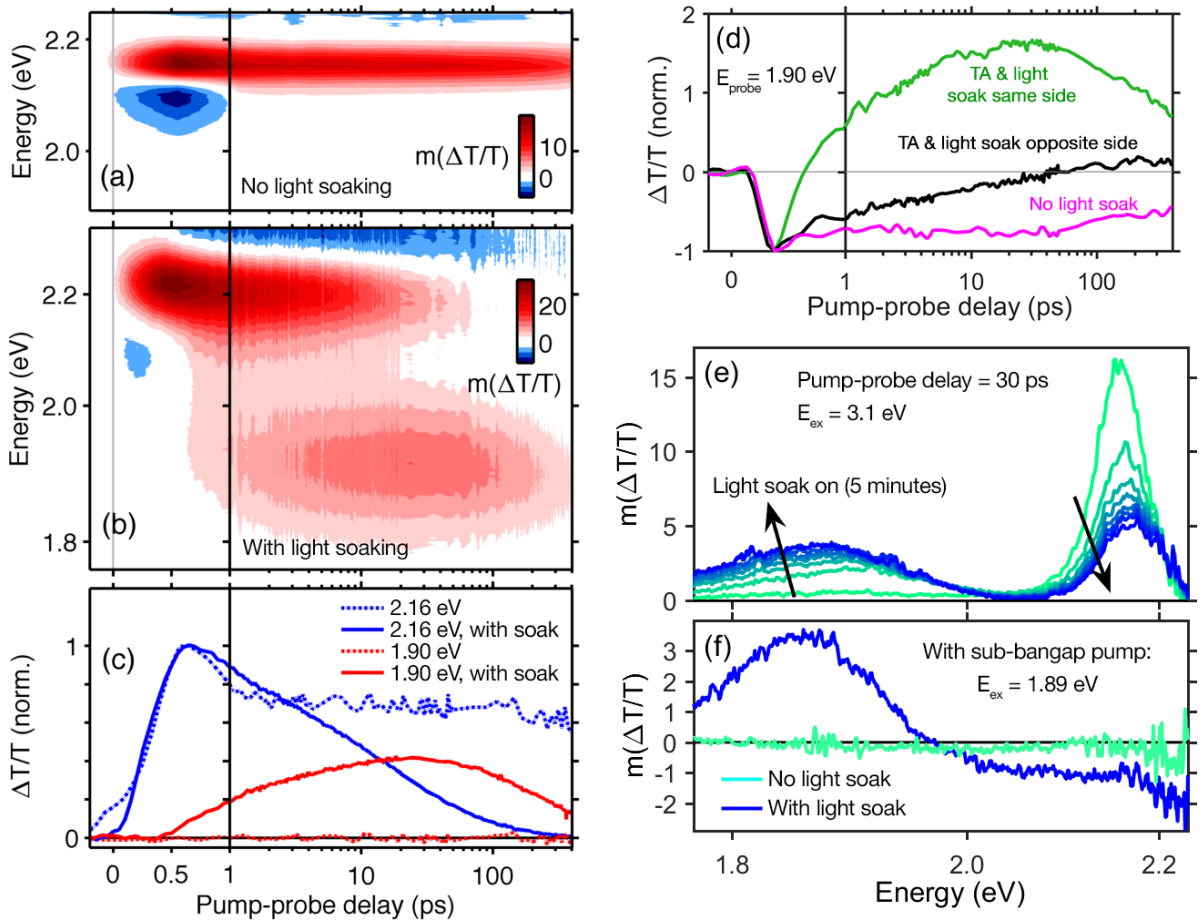


Figure 3: Ultrafast TA spectra of $MAPb(I_{0.15}Br_{0.85})_3$ perovskite thin film excited at 3.1 eV, (a) without and (b) with constant light bias (2.64 eV, 0.3 W/cm^2) . The kinetics of the low and high energy bleach features are shown in (c) both with and without light soaking. (d) Kinetics of the low energy bleach, with the light soaking & TA pulses illuminating either the same, or opposite surfaces of the sample. (e) Spectral evolution of the signal at a pump-probe delay of 30 ps upon light soaking. (f) TA spectra at a pump-probe delay of 30 ps for excitation at 1.88 eV, below the optical gap of the main blend.

Figure 3b shows the transient absorption map obtained when repeating the above experiment in the presence of above-gap light soaking (2.64 eV, 0.3 W/cm^2). Photoexcitation initially generates a single GSB as in Figure 3a. However, beginning at 0.5 ps, we see quenching of the main feature along with the concomitant emergence of a broad positive feature centred near 1.90 eV and extending to at least 1.77 eV similar to that previously reported by Yoon *et al.*[17] No similar photoinduced changes in the TA spectra were observed in pure tri-halide

perovskite samples (Figure S9). We attribute this feature to the relaxation of carriers from the pristine semiconductor to the sub-bandgap states formed under continuous wave (CW) light soaking. This process occurs extremely rapidly, with the sub-bandgap bleach rising to half of its maximum amplitude in ~1 ps. Under sufficient light soaking intensity, transfer to the sub-bandgap states can completely deplete the excited-state population in the pristine blend, a process that is complete within 100 ps for the data shown in Figure 3c. Unsurprisingly, the decay time of the quenched band-edge GSB is dependent on the intensity of light soaking. Figure S11 shows the GSB kinetics taken with a single TA pump power for a range of CW illumination intensities, with time constants decreasing from 91 ps at 0.15 W/cm^2 to 33 ps at 0.9 W/cm^2. Such dependence could be the result of luminescent site density increasing under more intense light soaking, however confocal mapping shows no indication of isolated iodide-rich sites on length scales larger than our spatial resolution (< 1 μm, Figure S10). The faster GSB quenching may alternatively be due to an increasing energetic gradient that enhances carrier collection.

We studied the formation of sub-bandgap states by fixing the TA pump-probe delay at 30 ps and observing the evolution of the spectral shape upon light soaking. As shown in Figure 3e, the sub-bandgap feature extends to lower energies as the photoinduced reorganization progresses, and is mirrored by a blue-shift of the above-gap feature, with both features becoming progressively broader. This behaviour is consistent with photoinduced halide segregation, with progressive enrichment/depletion of bromide fraction (and therefore local bandgap) for the regions corresponding to the above/sub-bandgap TA features, and a universal increase in energetic disorder. By reducing the energy of our pump pulses to 1.88 eV – below the bandgap of the pristine material – we are able to exclusively probe the sub-bandgap states. Figure 3f shows TA spectra at a pump-probe delay of 10 ps. In the absence of light soaking, no excited-state features are observed. Upon illumination, we obtain the isolated signal from the sub-bandgap states with no contribution from the band-edge,

supporting our assignment of the photoinduced absorption in Figure 1 to the formation of the iodide enriched material. The spectral shape strongly resembles that of a perovskite with smaller bandgap than our $MAPb(I_{0.15}Br_{0.85})_3$ blend, including the band-edge bleach and broad negative feature above the bandgap. In contrast to the above-gap excitation, with a 1.88 eV pump pulse the sub-bandgap bleach forms within the instrument response time (Figure S12), indicating direct excitation of the sub-bandgap states. It is revealing that Figure 3c shows no direct excitation of the sub-bandgap states, consistent with the photoinduced regions of low-bandgap perovskite comprising a very small fraction of the total sample, but dominating the PL by collecting carriers prior to recombination.

Figures 3a, b and c were collected with the pump, probe and light soak beams in an approximately collinear geometry, with each of the light sources illuminating the same face of the sample. By rearranging the light soak laser to illuminate the rear face of the sample, we can track the relaxation of photoinduced carriers that are generated in the 'dark' side of the film. Figure 3d shows that carriers generated on the opposite side of the (280 nm thick) film take significantly longer – tens rather than several ps – to relax to sub-bandgap states, and do so with a lower final yield. The increase in time required for carriers to experience and thermalise in to low-bandgap states indicates that the photoinduced iodide-rich regions of the sample are located close to the illuminated surface, where carrier generation rate is the highest.

Photo-induced structural modifications: XRD studies

We investigate the structural origin of the changes in the photo-physical properties of mixed-halide perovskites by analysing the light soaking induced changes in the crystal lattice with XRD measurements on thin spin-coated $MAPb(I_{1-x}Br_x)_3$ films (d ~ 200 nm). In contrast to the report of Hoke et al.[8] no new peaks were observed to form under WLB in any of the films studied. Figure 4 shows the X-ray diffraction (XRD) pattern for the (400) and (220) reflections of x = 0.6 and 0.4 perovskites as a function of time, upon application and

following removal of CW light soaking. In both the presence and absence of light soaking, the changes in $MAPb(I_{0.6}Br_{0.4})_3$ are observed to occur over a longer time period than in $MAPb(I_{0.4}Br_{0.6})_3$. This is consistent with observations of faster sub-bandgap PL growth rates with increasing bromide fraction.[8]

With light soaking we observe a shift of the peaks to higher 2θ due to a reduction in the unit cell volume. This is accompanied by a reduction in the intensity and a broadening of the reflections. On removal of light soaking the initial peak intensity and shape are recovered, with no change in the scattering angle, 2θ. Given the reversibility of the peak broadening, we attribute this to bulk strain rather than a reduction in crystallite size within the films.

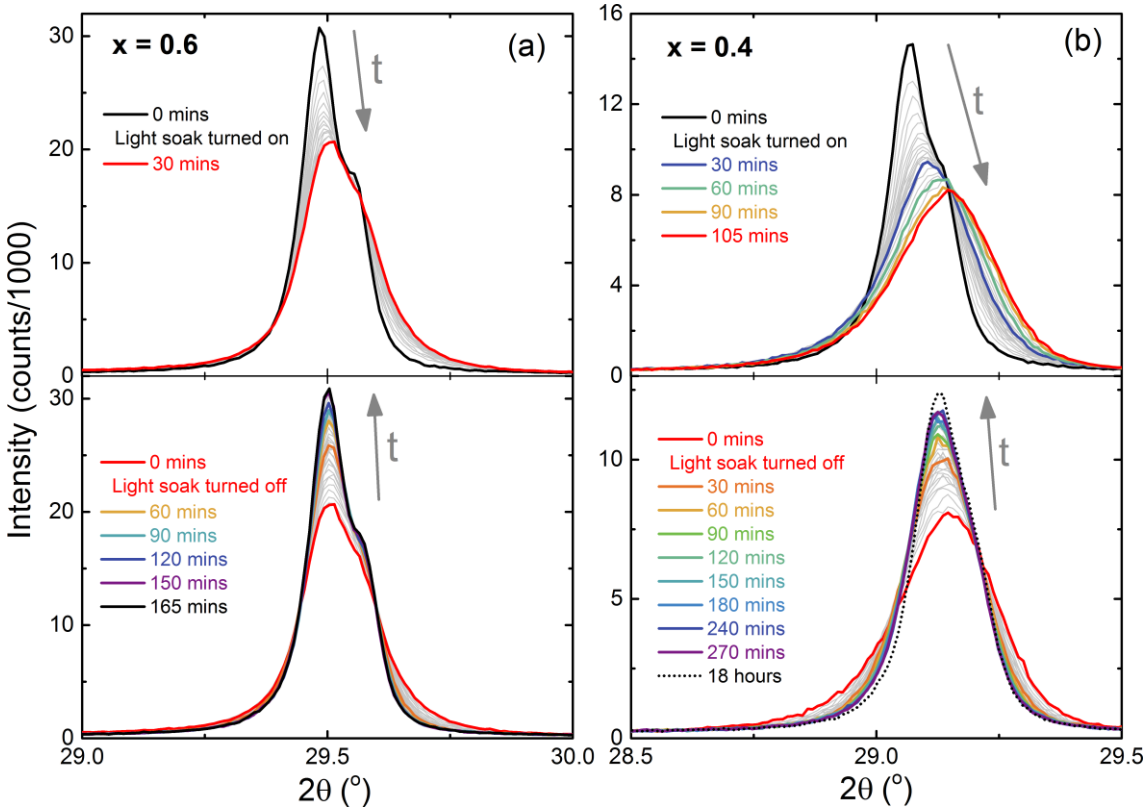


Figure 4: XRD patterns showing the time evolution of the (004) and (220) reflections for (a) $MAPb(I_{0.4}Br_{0.6})_3$ and (b) $MAPb(I_{0.6}Br_{0.4})_3$ under light soaking (top) and after removal of light soaking (bottom).

A Le Bail analysis[28] of the XRD data (Table S2) reveals that the photoinduced changes in the structure of the mixed-halide perovskites can be separated into three distinct regimes: 1. the

initial structure prior to light soaking; 2. (during soaking) a modified bulk structure with reduced volume, increased tetragonal distortion and increased strain; 3. (after light soaking is removed) a reduced volume phase with a small tetragonal distortion and low strain. The origin of the photoinduced changes in the XRD can thus be ascribed to at least two separate phenomena. Firstly, a reversible component arising from changes in the tetragonal distortion and strain that is associated with the reversible ion segregation and sub-bandgap PL. Secondly, an irreversible contraction of the unit cell volume upon initial light soaking, which could be a result of irreversible defect migration (such as the annihilation of halide vacancies and interstitials[29]).

XRD measurements of pure tri-bromide and tri-iodide perovskites did not show any changes to either the peak position or width (Figure S7). Additionally, temperature dependent XRD measurements did not replicate the above phenomena in any of the films (Figure S14), indicating that the photoinduced changes are due to the presence of charge carriers rather than localised sample heating.

Halide transport and the stability of intermixed vs. segregated configurations

To investigate the electronic properties of the $MAPbBr_3$/$MAPbI_3$ assembly and the possible ion migration across this interface we have built a model based on the best lattice matching between cubic $MAPbBr_3$ and tetragonal $MAPbI_3$. The employed model, reported in Figure 5a (details in SI), is based on a MABr-terminated 3x3x4 cubic $MAPbBr_3$ slab interfaced with a PbI_2-terminated 2x2x4 tetragonal $MAPbI_3$ slab. Such combination allows us to use the $MAPbI_3$ experimental cell parameters with a lattice mismatch with respect to $MAPbBr_3$ within 0.1%. The employed model shows nine terminal Br atoms (from $MAPbBr_3$) interfaced with 8 surface Pb atoms (from $MAPbI_3$). Upon geometry optimization, a total of 7 Br-Pb interfacial bonds are created, thus leading to an almost perfect saturation of under-coordinated interface atoms.

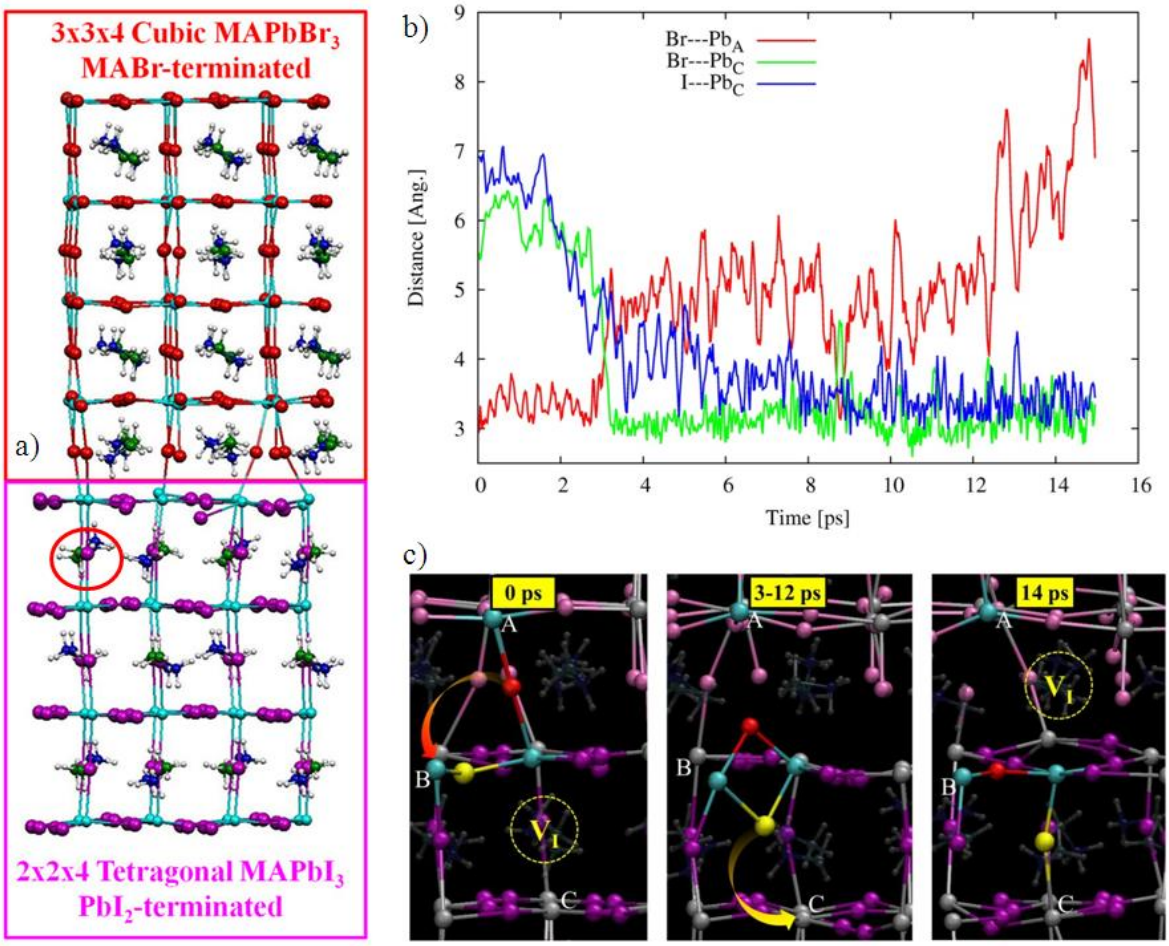


Figure 5: (a) Model of the MAPbBr3/MAPbI3 interface. The red circle in MAPbI3 indicates the site where an iodide vacancy is created. (b) Time evolution of the Pb-Br and Pb-I distances (see labels in left panel of Figure 3c). (c) Structural evolution following defect migration. At time = 0 an iodide vacancy is present in MAPbI3. At t = 3 ps a mixed I-Br split interstitial is formed, which is stable up to t = 12 ps. Afterwards (t = 14 ps), the iodide vacancy is transferred to the MAPbBr3 phase.

To investigate the possible ion migration across the $MAPbBr_3/MAPbI_3$ interface we subjected the model system of Figure 5a to *ab initio* molecular dynamics simulations; we heated up the system to 450 K and let it evolve in time for ~ 20 ps after a few ps of thermalisation. During this time we monitored the evolution of the interfacial bond lengths, but did not observe any ion migration, which is quite unlikely on the observed temperature and time range in an almost perfectly saturated system. The calculated activation energy for exchange of an iodide atom in bulk $MAPbI_3$ is ~ 0.5 eV (this process corresponds to 90° rotation of one PbI_6

octahedron along the *c* axis). This barrier is too high to be overcome during our relatively short dynamics simulations (on ps time scales) and is one order of magnitude higher than the activation energy associated with the photoinduced feature shown in impedance spectroscopy of mixed-halides (Figure S4).

We thus created an iodide vacancy in the second $MAPbI_3$ layer away from the interface (Figure 5a) and repeated the *ab initio* molecular dynamics simulations. By following the time evolution of the relevant geometrical parameters (Figure 5b) we observed migration of an interfacial Br^- ion within ~3 ps, as testified by the sudden increase of the Pb-Br distance corresponding to the initially bound couple (Figure 5b). Following this migration, a mixed I^-/Br^- split interstitial defect is created, leaving behind a Br^- vacancy in $MAPbBr_3$, which is stable for about 10 ps (3-12 ps range in Figure 5c). After this time, another migration event occurs, leading to incorporation of Br^- into the $MAPbI_3$ lattice and creation of a $MAPbBr_3$ bromide vacancy (14 ps range in Figure 5c). The driving force for defect migration is probably the slight halide imbalance at the interface (9 Br atoms which bind to 8 Pb centres) but we cannot exclude a Br^- vacancy stabilization compared to formation of an I^- vacancy. The observed relatively short time for vacancy migration is consistent with the recently reported activation energies for such processes, which amounts to ~ 0.1 eV for $MAPbI_3$, with bromide vacancy migration in $MAPbBr_3$ featuring a reduced activation energy.[30,31]

To check whether a halide-segregated phase could be stabilized by light absorption with respect to a dispersed phase in the absence of defects, we considered two bulk systems with the same 3:1 I:Br stoichiometry but with bromide either evenly dispersed or concentrated in a specific region (Figure S19). To approximately simulate the effect of light absorption, we considered here the lowest triplet excited state of both systems. Notably, in both the ground and excited state the Br-dispersed phase is more stable than the Br-concentrated phase by 0.13 and 0.06 eV, respectively. Thus, our simulations performed on perfectly crystalline bulk

phases do show an energy gain associated to halide segregation although the driving force for this process is not sufficient alone to stabilize the phase segregated phase.

Overall, our computational analyses suggest that halide defects, typically halide vacancies and interstitials, promote halide migration by providing low-energy migration pathways. Notably, the defect assisted halide migration in $MAPbI_3$ was proposed to be activated by light, [28] in line with the present observations.

Discussion: Photoinduced halide segregation and methods of passivation

Recent investigations of the mechanics of the Hoke effect have ascribed its origin to polaron formation, or a miscibility gap of the solid mixed-halide solution due to changes in the Helmholz free energy upon photoexcitation.[9,11,15] While our calculations do indicate partial stabilisation of the halide-segregated configuration under illumination, the existing models do not explain our observed dependence of the Hoke effect on illumination wavelength, excitation geometry, and film thickness. These effects imply the role of an internal gradient in light intensity (and therefore carrier generation rate) in driving halide segregation, so we consider here a mechanism by which such a gradient may contribute to the Hoke effect.

The internal gradient in carrier generation rate may induce ion migration *via* the photoinduced strain gradient in the lattice indicated in our XRD results, or more directly, for example with the excess energy from hot carriers thermalising near the illuminated surface providing energy to activate halide defects (with calculated values of 50 meV deposited from carriers to each molecule at the surface of a film under solar illumination[32]). We do not consider that the effect is due to bulk heating of the sample; experiments that applied a temperature gradient across the sample were unable to induce halide segregation (Figure S14 & Figure S15).

Results in the literature support the role of light gradients in affecting ion migration: deQuilletes *et al* have demonstrated iodide migration away from illuminated regions in $MAPbI_3$, and ion drift velocities in thin films of $MAPbI_3$ have been shown to increase substantially under illumination.[33] If halide anions are more mobile near the illuminated

surface, this would result in net transport down into the film, migrating *via* halide defect sites. In a mixed-halide, any difference in hopping rate between bromide and iodide would result in a vertical gradient of iodide:bromide ratio and therefore of local bandgap. Carriers generated in the resulting material will be funnelled to the lowest energy region,[34,35] recombining to generate the sub-bandgap PL characteristic of the Hoke effect. The slower relaxation of carriers generated opposite the illuminated face in Figure 3d reveal that the iodide-rich low-bandgap region is located at the illuminated surface of the film, corresponding to faster migration of bromide in the vertical segregation model.

Once carriers are funnelled to the low-bandgap regions, the rate of non-radiative recombination is lower due to local enhancement of carrier density, which fills traps and increases bimolecular recombination, explaining the much higher intensity of the sub-bandgap PL compared with the pristine blend. Specifically, although PDS (Figure 1a) shows that sub-bandgap regions comprise <5% of sample volume, they can fully capture all excitations in less than the radiative lifetime (Figure 3c), implying at least 20-fold increase in local carrier density.

When CW illumination (or the internal light gradient, as in Figure 2b) is removed, the vertical gradient in carrier generation rate disappears and the sample undergoes remixing to the homogeneous state, albeit at a slower rate,[17] possibly since ion mobilities are reduced in the dark.[33] Our calculations show that this intermixing is entropically-driven, with the homogeneously mixed state being energetically favourable (by 0.11 eV in our model). This may work in tandem with the proposed driving force for remixing due to differences in the free energy of mixing in the presence of carriers.[11]

Our computational investigations show that ion migration in mixed-halide systems takes place *via* halide defects. Consistently, Figure 1 shows that a film prepared with a large excess of the halide-bearing precursors does not exhibit the Hoke effect. The abundance of halide ions available during film crystallisation should result in a film with reduced halide vacancies, thus

lowering ion mobility. Furthermore, both the absorption and PL show higher disorder than the stoichiometric films, which we attribute to spatial variations in halide ratio being 'frozen in' during film formation. The low density of halide vacancies would preclude the entropy-driven halide intermixing process that takes place in the dark, and which is likely the origin of improvements in film homogeneity that have been observed to take place after initial film preparation in stoichiometric mixed-halide films.[6]

These results explain the absence of photoinduced sub-bandgap states in mixed-halide nanocrystals[14] which benefit doubly, having both low halide defect density and negligible difference in carrier generation rate across a given crystal.

The final piece of this puzzle is the independence of sub-bandgap PL energy on initial halide ratio, sample preparation and light intensity. This energy — 1.68 eV — corresponds to a mixed-halide sample with a composition of $x \approx 0.20$.[36] This value is coincident with a tetragonal-to-cubic phase transition reported by Noh and co-workers[5] as lying between $x = 0.13$ and $x = 0.2$. It is possible that bromide depletion at the illuminated surface proceeds until $x \approx 0.20$, beyond which the lattice phase transition presents an energetic barrier to further depletion, determining the final energy of the sub-bandgap emission. Indeed, the existence of a stable alloy at room temperature with ratio $x < 0.19$ has been predicted from thermodynamic analysis,[9] and is consistent with ratios that have been empirically determined to provide stable performance when used in photovoltaic devices.[5,37]

It is important to note that many of the factors governing the strength of the Hoke effect – such as illumination intensity, sample history, use of an excess of halide precursor or mixed A-site cations – have also been shown to correlate with the stability of the intensely studied tri-iodide perovskites, in particular with the degree of hysteresis observed in device performance.

Confidence in the attribution of both the Hoke effect and hysteresis in tri-halide devices to ion migration continues to grow with the rapid rate of publication on these materials. Indeed, it is

possible that the underlying processes are due to similar mechanisms, and that the presence of two mobile anions with different mobilities along with the strong dependence of material bandgap on local halide ratio simply provides a sensitive photoluminescent tag revealing ion migration in mixed-halide perovskites. For these reasons, understanding – and controlling – the Hoke effect may guide improvements in the stability not just of tuneable and high-bandgap materials, but of organolead halide perovskites in general.

In summary, our results on the structural and photophysical properties of mixed lead-halide perovskites are in agreement with defect-assisted migration of halide ions away from the film surface. It is possible that this migration is a result of the steep carrier generation gradient that exists during illumination. In this model, the slower hopping rate of iodide results in bromide depletion to a final composition of $MAPb(I_{0.8}Br_{0.2})_3$, where a cubic-to-tetragonal phase transition prevents further segregation, determining the 1.68 eV energy of the final photoinduced sub-bandgap emission.

The ability to control or prevent photoinduced halide segregation will be crucial to realising tuneable mixed-halide optoelectronic devices. We have demonstrated both structural and compositional approaches using film thickness and precursor ratio to alter the susceptibility of mixed-halide films to ion segregation. In addition, the use of colloidal perovskite crystals — which exhibit both low defect density and low carrier generation inhomogeneity — may provide a useful avenue for the creation of stable tuneable devices. Indeed, sufficient control of spatial differences in halide ratio may even enable the creation of multi-level systems for applications such as lasing, as has been demonstrated recently[38] by exploiting temperature-dependent phase transitions in $MAPbI_3$. Furthermore, mixed-halide systems — and the stabilisation methods presented here — have direct relevance to the more intensely studied family of tri-halide perovskites (such as $MAPbI_3$), which feature the same photoinduced halide migration processes, but lack the clear photoluminescent indicator of migration described in this work.

Acknowledgements
We acknowledge funding from the Engineering and Physical Sciences Research Council (EPSRC) and the Winton Programme (Cambridge) for the Physics of Sustainability. The research leading to these results has received funding from the European Union Seventh Framework Programme (FP7/2007-2013) under grant agreement no. 604032 of the MESO project. A.S. acknowledges the funding and support from the Indo-UK APEX project. F.D. acknowledges funding from Herchel Smith fellowship. SPS acknowledges funding from the Royal Society for the Newton International Fellowship. A.J.P. thanks David Lidzey (University of Sheffield) for use of a sample chamber for GIWAXS measurements. We thank Diamond Light Source for access to beamlines I12 and I07 (sessions EE11454-1 and SI12436-1 respectively) that contributed to the results presented here. We thank Prof. Paul Bristowe, Prof. Aron Walsh, Dr. Jung-Hoon Lee, and Dr. James Ball for helpful discussions.

Supporting Information Available: Experimental and computational methods, Le Bail analysis of XRD, temperature-dependent impedance spectroscopy, additional structural (XRD, WAXS, GIWAXS) and optical (ultrafast TA, PL, confocal PL mapping) characterisation of mixed- and tri-halide samples including at low temperature, with applied heat gradients, and of caesium lead mixed-halide perovskite.

References

(1) NREL. Best Research-Cell Efficiencies. https://www.nrel.gov/pv/assets/images/efficiency-chart.png (Accessed 1st April 2017).
(2) Deschler, F.; Price, M.; Pathak, S.; Klintberg, L. E.; Jarausch, D.-D.; Higler, R.; Hüttner, S.; Leijtens, T.; Stranks, S. D.; Snaith, H. J.; *et al.* High Photoluminescence Efficiency and Optically Pumped Lasing in Solution-Processed Mixed Halide Perovskite Semiconductors. *J. Phys. Chem. Lett.* **2014**, *5*, 1421–1426.
(3) Cho, H.; Jeong, S.-H.; Park, M.-H.; Kim, Y.-H.; Wolf, C.; Lee, C.-L.; Heo, J. H.; Sadhanala, A.; Myoung, N.; Yoo, S.; *et al.* Overcoming the electroluminescence efficiency limitations of perovskite light-emitting diodes. *Science* **2015**, *350*, 1222–1225.
(4) Sadhanala, A.; Ahmad, S.; Zhao, B.; Giesbrecht, N.; Pearce, P. M.; Deschler, F.; Hoye, R. L. Z.; Gödel, K. C.; Bein, T.; Docampo, P.; *et al.* Blue-Green Color Tunable Solution Processable Organolead Chloride–Bromide Mixed Halide Perovskites for Optoelectronic Applications. *Nano Lett.* **2015**, *15*, 6095–6101.
(5) Noh, J. H.; Im, S. H.; Heo, J. H.; Mandal, T. N.; Seok, S. Il. Chemical Management for Colorful, Efficient, and Stable Inorganic–Organic Hybrid Nanostructured Solar Cells. *Nano Lett.* **2013**, *13*, 1764–1769.
(6) Sadhanala, A.; Deschler, F.; Thomas, T. H.; Dutton, S. E.; Goedel, K. C.; Hanusch, F. C.; Lai, M. L.; Steiner, U.; Bein, T.; Docampo, P.; *et al.* Preparation of Single-Phase Films of $CH_3NH_3Pb(I_{1-x}Br_x)_3$ with Sharp Optical Band Edges. *J. Phys. Chem. Lett.* **2014**, *5*, 2501–2505.
(7) Gil-Escrig, L.; Miquel-Sempere, A.; Sessolo, M.; Bolink, H. J. Mixed Iodide–Bromide Methylammonium Lead Perovskite-based Diodes for Light Emission and Photovoltaics. *J. Phys. Chem. Lett.* **2015**, *6*, 3743–3748.
(8) Hoke, E. T.; Slotcavage, D. J.; Dohner, E. R.; Bowring, A. R.; Karunadasa, H. I.; McGehee, M. D. Reversible photo-induced trap formation in mixed-halide hybrid perovskites for photovoltaics. *Chem. Sci.* **2015**, *6*, 613–617.
(9) Brivio, F.; Caetano, C.; Walsh, A. Thermodynamic Origin of Photoinstability in the $CH_3NH_3Pb(I_{1-x}Br_x)_3$ Hybrid Halide Perovskite Alloy. *J. Phys. Chem. Lett.* **2016**, *7*,

1083–1087.
(10) Slotcavage, D. J.; Karunadasa, H. I.; McGehee, M. D. Light-Induced Phase Segregation in Halide-Perovskite Absorbers. *ACS Energy Lett.* **2016**, 1199–1205.
(11) Bischak, C. G.; Hetherington, C. L.; Wu, H.; Aloni, S.; Ogletree, D. F.; Limmer, D. T.; Ginsberg, N. S. Origin of Reversible Photoinduced Phase Separation in Hybrid Perovskites. *Nano Lett.* **2017**, *17*, 1028–1033.
(12) McMeekin, D. P.; Sadoughi, G.; Rehman, W.; Eperon, G. E.; Saliba, M.; Horantner, M. T.; Haghighirad, A.; Sakai, N.; Korte, L.; Rech, B.; *et al.* A mixed-cation lead mixed-halide perovskite absorber for tandem solar cells. *Science* **2016**, *351*, 151–155.
(13) Beal, R. E.; Slotcavage, D. J.; Leijtens, T.; Bowring, A. R.; Belisle, R. A.; Nguyen, W. H.; Burkhard, G.; Hoke, E. T.; McGehee, M. D. Cesium lead halide perovskites with improved stability for tandem solar cells. *J. Phys. Chem. Lett.* **2016**, 746–751.
(14) Akkerman, Q. A.; D'Innocenzo, V.; Accornero, S.; Scarpellini, A.; Petrozza, A.; Prato, M.; Manna, L. Tuning the Optical Properties of Cesium Lead Halide Perovskite Nanocrystals by Anion Exchange Reactions. *J. Am. Chem. Soc.* **2015**, *137*, 10276–10281.
(15) Slotcavage, D. J.; Karunadasa, H. I.; McGehee, M. D. Light-Induced Phase Segregation in Halide-Perovskite Absorbers. *ACS Energy Lett.* **2016**, *1*, 1199–1205.
(16) Yang, X.; Yan, X.; Wang, W.; Zhu, X.; Li, H.; Ma, W.; Sheng, C. Light induced metastable modification of optical properties in $CH_3NH_3PbI_{3-x}Br_x$ perovskite films: Two-step mechanism. *Org. Electron.* **2016**, *34*, 79–83.
(17) Yoon, S. J.; Draguta, S.; Manser, J. S.; Sharia, O.; Schneider, W. F.; Kuno, M.; Kamat, P. V. Tracking Iodide and Bromide Ion Segregation in Mixed Halide Lead Perovskites during Photoirradiation. *ACS Energy Lett.* **2016**, *1*, 290–296.
(18) Jaffe, A.; Lin, Y.; Beavers, C. M.; Voss, J.; Mao, W. L.; Karunadasa, H. I. High-Pressure Single-Crystal Structures of 3D Lead-Halide Hybrid Perovskites and Pressure Effects on their Electronic and Optical Properties. *ACS Cent. Sci.* **2016**, *2*, 201–209.
(19) Tian, Y.; Peter, M.; Unger, E.; Abdellah, M.; Zheng, K.; Pullerits, T.; Yartsev, A.; Sundström, V.; Scheblykin, I. G. Mechanistic insights into perovskite photoluminescence enhancement: light curing with oxygen can boost yield thousandfold. *Phys. Chem. Chem. Phys.* **2015**, *17*, 24978–24987.
(20) Snaith, H. J.; Abate, A.; Ball, J. M.; Eperon, G. E.; Leijtens, T.; Noel, N. K.; Stranks, S. D.; Wang, J. T.-W.; Wojciechowski, K.; Zhang, W. Anomalous Hysteresis in Perovskite Solar Cells. *J. Phys. Chem. Lett.* **2014**, *5*, 1511–1515.
(21) Leijtens, T.; Stranks, S. D.; Eperon, G. E.; Lindblad, R.; Johansson, E. M. J.; McPherson, I. J.; Rensmo, H.; Ball, J. M.; Lee, M. M.; Snaith, H. J. Electronic Properties of Meso-Superstructured and Planar Organometal Halide Perovskite Films: Charge Trapping, Photodoping, and Carrier Mobility. *ACS Nano* **2014**, *8*, 7147–7155.
(22) Yoon, S.; Stamplecoskie, K. G.; Kamat, P. V. How Lead Halide Complex Chemistry Dictates the Composition of Mixed Halide Perovskites. *J. Phys. Chem. Lett.* **2016**, 1368–1373.
(23) Lin, Q.; Armin, A.; Nagiri, R. C. R.; Burn, P. L.; Meredith, P. Electro-optics of perovskite solar cells. *Nat. Photonics* **2014**, *9*, 106–112.
(24) Manser, J. S.; Kamat, P. V. Band filling with free charge carriers in organometal halide perovskites. *Nat. Photonics* **2014**, *8*, 737–743.
(25) Grancini, G.; Srimath Kandada, A. R.; Frost, J. M.; Barker, A. J.; De Bastiani, M.; Gandini, M.; Marras, S.; Lanzani, G.; Walsh, A.; Petrozza, A. Role of microstructure in the electron–hole interaction of hybrid lead halide perovskites. *Nat. Photonics* **2015**, *9*, 695–701.
(26) Price, M. B.; Butkus, J.; Jellicoe, T. C.; Sadhanala, A.; Briane, A.; Halpert, J. E.; Broch, K.; Hodgkiss, J. M.; Friend, R. H.; Deschler, F. Hot-carrier cooling and photoinduced

refractive index changes in organic–inorganic lead halide perovskites. *Nat. Commun.* **2015**, *6*, 8420.
(27) Chen, K.; Barker, A. J.; Morgan, F. L. C.; Halpert, J. E.; Hodgkiss, J. M. Effect of Carrier Thermalization Dynamics on Light Emission and Amplification in Organometal Halide Perovskites. *J. Phys. Chem. Lett.* **2015**, *6*, 153–158.
(28) Le Bail, A.; Duroy, H.; Fourquet, J. L. Ab-initio structure determination of LiSbWO6 by X-ray powder diffraction. *Mater. Res. Bull.* **1988**, *23*, 447–452.
(29) Mosconi, E.; Meggiolaro, D.; Snaith, H. J.; Stranks, S. D.; De Angelis, F. Light-induced annihilation of Frenkel defects in organo-lead halide perovskites. *Energy Environ. Sci.* **2016**, *9*, 3180–3187.
(30) Azpiroz, J. M.; Mosconi, E.; Bisquert, J.; De Angelis, F. Defect migration in methylammonium lead iodide and its role in perovskite solar cell operation. *Energy Environ. Sci.* **2015**, *8*, 2118–2127.
(31) Meloni, S.; Moehl, T.; Tress, W.; Franckevičius, M.; Saliba, M.; Lee, Y. H.; Gao, P.; Nazeeruddin, M. K.; Zakeeruddin, S. M.; Rothlisberger, U.; *et al.* Ionic polarization-induced current–voltage hysteresis in $CH_3NH_3PbX_3$ perovskite solar cells. *Nat. Commun.* **2016**, *7*, 10334.
(32) Liu, S.; Zheng, F.; Grinberg, I.; Rappe, A. M. Photoferroelectric and Photopiezoelectric Properties of Organometal Halide Perovskites. *J. Phys. Chem. Lett.* **2016**, *7*, 1460–1465.
(33) Xing, J.; Wang, Q.; Dong, Q.; Yuan, Y.; Fang, Y.; Huang, J. Ultrafast ion migration in hybrid perovskite polycrystalline thin films under light and suppression in single crystals. *Phys. Chem. Chem. Phys.* **2016**, *18*, 30484–30490.
(34) Yuan, M.; Quan, L. N.; Comin, R.; Walters, G.; Sabatini, R.; Voznyy, O.; Hoogland, S.; Zhao, Y.; Beauregard, E. M.; Kanjanaboos, P.; *et al.* Perovskite energy funnels for efficient light-emitting diodes. *Nat. Nanotechnol.* **2016**, *11*, 872–877.
(35) Tian, W.; Leng, J.; Zhao, C.; Jin, S. Long-Distance Charge Carrier Funneling in Perovskite Nanowires Enabled by Built-in Halide Gradient. *J. Am. Chem. Soc.* **2017**, *139*, 579–582.
(36) Jesper Jacobsson, T.; Correa-Baena, J.-P.; Pazoki, M.; Saliba, M.; Schenk, K.; Grätzel, M.; Hagfeldt, A. Exploration of the compositional space for mixed lead halogen perovskites for high efficiency solar cells. *Energy Environ. Sci.* **2016**, *9*, 1706–1724.
(37) Jeon, N. J.; Noh, J. H.; Yang, W. S.; Kim, Y. C.; Ryu, S.; Seo, J.; Seok, S. Il. Compositional engineering of perovskite materials for high-performance solar cells. *Nature* **2015**, *517*, 476–480.
(38) Neutzner, S.; Srimath Kandada, A. R.; Lanzani, G.; Petrozza, A. A dual-phase architecture for efficient amplified spontaneous emission in lead iodide perovskites. *J. Mater. Chem. C* **2016**, *4*, 4630–4633.